Materials International
Open Access Journal (ISSN: 2668-5728)

Article
Volume 4, Issue 1, 2022, 5
https://doi.org/10.33263/Materials41.005

Elaboration of a Model System Multilayered Si (substrate)/TiFe/Zr/Pd Thin Film by Magnetron Sputtering

Volatiana Razafindramanana [1,2], Lionel Teulé-Gay [1], Jacques Huot [2], Jean-Louis Bobet [1,*]

[1] Université de Bordeaux, Institut de chimie de la matière condensée de Bordeaux, Pessac 33600, France;
[2] Université du Québec à Trois-Rivières, Institut de Recherche sur l'Hydrogène, Trois Rivières, Québec, Canada;
* Correspondence: Jean-louis.bobet@u-bordeaux.fr (J.L.B.);

Scopus Author ID 7004912456
Received: 10.01.2022; Accepted: 15.02.2022; Published: 9.03.2022

Abstract: A model system of a tri-layered 60 nm TiFe / 10 nm Zr / 5 nm Pd thin film on (100) oriented Si substrate was deposited by magnetron sputtering. The iron-titanium layer was sputtered by co-sputtered mode. Depending on the power per unit area of each component and the substrate temperature, the stoichiometry Ti:Fe oscillates between 1:2 and 1:1. Sample characterization by electron probe microanalyzer (EPMA) and X-ray photoelectron spectroscopy (XPS) indicates that the composition Fe_1Ti_1 is obtained with a total power of 80W (*i.e.*, 1.81W/cm²) for Fe and 60W (*i.e.*, 1.36W/cm²) for Ti. Grazing incident X-ray diffraction analysis shows that the as-deposited TiFe is well crystallized with a CsCl structure. Palladium covers all the TiFe/Zr film, but zirconium seems to be amorphous. The deuterium absorption loss caused by oxygen contamination is presented.

Keywords: hydrogen; thin film; FeTi.

© 2022 by the authors. This article is an open-access article distributed under the terms and conditions of the Creative Commons Attribution (CC BY) license (https://creativecommons.org/licenses/by/4.0/).

1. Introduction

The intermetallic compound TiFe is an interesting hydrogen storage material since it has a low production cost and can store hydrogen reversibly at room temperature [1]. However, the first hydrogen absorption, the so-called activation process, is arduous due to passivating surface oxidation that stops or delays hydrogen diffusion in the compound [2-4]. Moreover, this compound has problems of corrosion that can be solved by coating the TiFe surface with an H_2 permeable and non-corrosive material [5].

To break the oxide layer, several cycles must be done at high pressure and high temperature [1]. However, such a procedure could be time-consuming and costly for the industrial-size synthesis of the alloy. Since the '80s, several works have been done to minimize these conditions of the activation process by partial substitution of one of the two elements with Al, Cr, Mn, Zr, or Ni [6-12], or by adding a dopant such as S, Pd, Zr or Ni [13-15] or by mechanical alloying [16-20]. Most of these works showed that a third metallic compound in TiFe induces the creation of a secondary phase rich in this third element. In previous work, hafnium (Hf), present in industrial-grade zirconium (Zr), has been shown to improve the first hydrogenation process of TiFe alloy [23]. The addition of hafnium, and so zirconium, induces the formation of two Hf-rich secondary phases in addition to the main B2-TiFe phase: Fe-rich Laves-C14 and Ti-rich BCC. The solidification path using the Scheil-Gulliver simulation confirmed this observation.

The hydrogen diffusion occurs first through the Hf-rich secondary phase then into the TiFe matrix. The interface between these two phases between Hf and TiFe is an important key to understanding the hydrogenation process.

This paper reports the investigation of the synthesis of TiFe/Zr/Pd trilayers on Si (100) wafers. Zirconium has been chosen as a dopant due to its lower cost than hafnium. This could be the first step to understand why the activation process is facilitated by the presence of zirconium (or hafnium) and to study the interface between the matrix and the dopant. The synthesis of this model material with very precise control of the composition is then of prime importance because such a layered system may serve as a model system to investigate the zirconium diffusion in the TiFe layer and the hydrogen diffusion in the tri-layers. The incidence of oxygen contamination, for example, should be addressed very carefully. The synthesis was made on a silicon wafer. A TiFe layer was deposited, followed by a zirconium layer, and topped with a palladium layer, which protects against oxidation and provides dissociation of molecular hydrogen [5,13,21].

2. Materials and Methods

2.1. Sample preparation.

Tri-layers TiFe/Zr/Pd on (100) oriented commercial silicon wafers (1 * 1 cm) as substrate was synthesized using a high-vacuum chamber magnetron sputtering apparatus. Due to the different sizes of our targets, two different chambers were used: one equipped with 3 inches targets in co-sputtering configuration (MP700), the other with 2 inches target magnetron sputtering (Leybold Heraeus).

Targets consisted of disks of pure Fe, Ti, Zr, Pd from Neyco (purity> 99,99%). 13.56 MHz radiofrequency supplies independently powered each target. Both chambers were pumped down to pressure below $3{,}5x10^{-7}$ Pa before sputtering. The films were elaborated under an Ar flow (Dinal Alphagaz 2>99.999% purified through an R.D. Mathis purifier: titanium heated at 600 °C) at a pressure of 0.5 Pa. During co-sputtering, the substrate holder was rotated to make a homogeneous thin film. Before each synthesis, and etching (Ar) of 3 minutes was done with an Anatech IS 3000 ion source to eliminate oxidation pollution at the substrate surface with impinging. The film deposition rate (for larger deposition thickness) was determined by mechanical profilometry using a Dektak instrument.

To obtain a layer of TiFe, a target made of TiFe alloy was first used in a normal sputtering mode. However, they have different deposition speeds even if Ti and Fe have a close vaporization temperature (2861°C for Fe and 3287°C for Ti). Hence, it was impossible to have a ratio of 50:50 of the two elements in the sputtered layer. Thus, two targets of Fe (purity 99.9%) and Ti (purity 99.9%) were required and were sputtered at the same time (co-sputtering mode).

Many sputtering parameters influence the composition, so we have focused on the target's RF power, substrate temperature, and time deposition to have the right composition and optimum thickness.

Ti and Fe's deposition parameters were fixed to obtain the right stoichiometry and a layer close to 50 (±10) nm. The Ti power was fixed at 60 W/cm^{2,} and Fe power was varied between 80 and 165 W/cm^2 to obtain a Fe/Ti film composition close to 50/50. The Fe and Ti target was pre-sputtered for 45 minutes to stabilize the surface composition. The substrate temperature during the sputtering was varied from 550°C to 650°C to promote the

crystallization of the TiFe phase. Zirconium was deposited in the same chamber (Plassys MP700) as iron and titanium, with the same sputtering conditions with a power of 10 W/cm^2 to reach a thickness of 10 (±5) nm. A thin layer (10 (±5) nm) of palladium was deposited to avoid oxidation of the hydrogen storage film underneath it and to dissociate the hydrogen molecules at the surface catalytically. By lack of means, the palladium was deposited in another chamber (Leybold Heraeus) at room temperature. The transfer time was less than 2 minutes in the air. A supplementary etching was realized to eliminate the residual oxides at the surface that occurred during the transfer. The thickness of each layer was optimized depending on the deposition time and sputtering conditions. The details of the sputtering conditions of the TiFe/Zr/Pd thin films are summarized in Table 1.

Table 1. Sputtering conditions for FeTi/Zr/Pd film preparation.

Target material	**Fe**	**Ti**	**Zr-Pd**
Initial pressure in chamber (Pa)	$3.5x10^{-7}$	$3.5x10^{-7}$	$3.5x10^{-7}$
Sputtering gas	Ar	Ar	Ar
Sputtering pressure (Pa)	0.5	0.5	0.5
Target-substrate distance (mm)	110	110	80
Substrate temperature (°C)	RT-550-600	RT-550-600	RT
Power per unit area (W/cm^2)	80 to 165	60	10

2.2. Characterization of the tri-layer TiFe/Zr/Pd.

Hydrogen absorption was characterized by neutron reflectometry. This analysis was performed on the D3 reflectometer at the neutron research reactor NRU in Chalk River. More technical details are presented elsewhere [22]. The used neutron wavelength was 0.237 nm. The measurement was performed in: (a) as-sputtered condition; (b) *in-situ* at room temperature under a deuterium pressure (P_D) of 10 mbar; and (c) *in-situ* at room temperature under a P_D = 500 mbar, using an ultra-high purity deuterium (i.e. 99.999%). In those experiments, deuterium was used instead of hydrogen because of the large incoherent scattering of hydrogen.

An Electron Probe MicroAnalyzer (EPMA-CAMECA SX 100 with a probe depth of 1 μm^3), and Rutherford Backscattering Spectrometry (RBS) analysis done at the Center of Nuclear Studies of Bordeaux-Gradignan (CENBG), examined the composition and the homogeneity of the as-deposited film samples. For RBS, a 2 MeV helium $4He^+$ beam was directed at the sample, and the energy of the backscattered helium ions is measured at a scattering angle of 5°. The ions lose energy through electronic and nuclear stopping through the sample, i.e., by interaction with the electron clouds around the target atoms. The energy loss depends on the stopping cross-section of the nucleus and, thus, on its mass and atomic number. The layer's thicknesses were determined from Auger electron spectroscopy (Auger VG Microlab 310F) with a depth resolution of 5 nm and a probe diameter of 20 nm and using a sputtering rate of 0.04 nm/s. With this technique, the depth profiles of each element present in the multilayer were measured. X-ray photoelectron spectroscopy (VG ESCALAB 220i-XL) was used to complement Auger electron spectroscopy to analyze the evolution of the elements' chemical environment, especially zirconium. The crystal structure of the tri-layer was probed by grazing incidence X-ray diffraction at different angles (0.3-0.6-1.0 and 1.5°) using a high-resolution diffractometer (Bruker D8 Discover) with Cu-Kα radiation.

3. Results and Discussion

3.1. TiFe layer synthesis.

According to previous experiments, the power per unit area of titanium was fixed at 60 W/cm², as it corresponds to the suitable deposition rate. Then we tried to adjust the power of the iron target.

Different values (80, 100, 120, and 165) of power per unit area of the iron target were investigated. The effect of this variation on the proportion of Fe/Ti measured by EPMA is shown in Fig. 1. The lower the power, the more Fe/Ti proportion approaches the ideal composition 1Fe-1Ti. The composition 1Fe-1Ti was observed with a power per unit area of 80W/cm^2 for iron and 60W/cm^2 for titanium. In these sputtering conditions and thanks to the rotation of the sample holder, the film was homogeneous on the substrate surface, as shown in Figure 2 by electron microprobe analyzer. The average composition of the film was 49.8Fe-50.2Ti, with a standard deviation of 0.2.

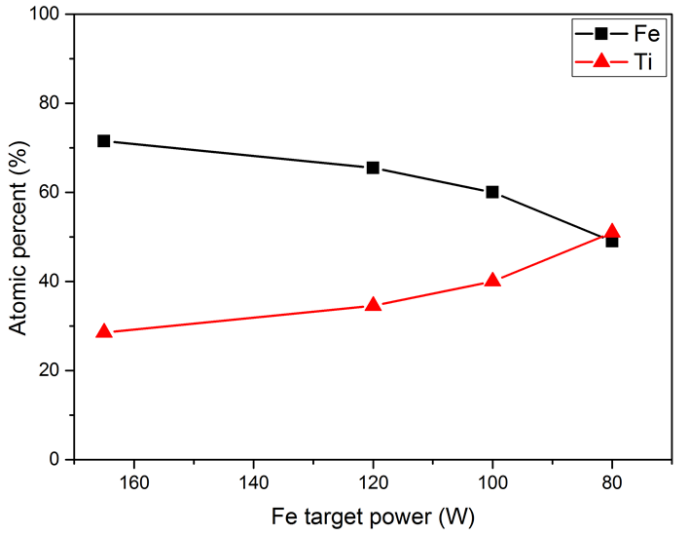

Figure 1. Atomic percent of Fe and Ti measured by EPMA in the function of the power per unit of Fe.

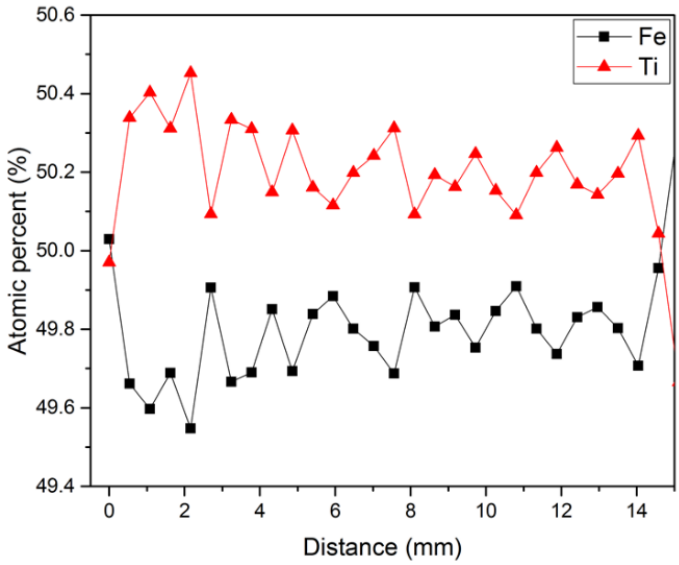

Figure 2. Surfacing analysis of the atomic percent of Fe and Ti. Substrate temperature: 550°C, P_{Fe} =80 W, and P_{Ti}=60 W.

3.2. TiFe layer structural analysis.

Rutherford Backscattering Spectrometry (RBS) analysis was done on samples prepared at 550, 600, and 650°C. Fig 3 shows a typical RBS data of a TiFe thin film on Si substrate. The zoom between 500 and 600 channels correspond to the interface substrate -layer. The zoom shows a different slope for the sample prepared at 650°C compared to those prepared at 550 and 600°C. After analysis with the SIMNRA program, this slope corresponds to a mixture of Fe, Ti, and Si with a composition of $FeTiSi_2$. Hence, we can affirm diffusion at the interface substrate/layer at 650°C. A small difference between 550 and 600°C is slightly visible with RBS analysis. The two peaks observed at channels 725 and 758 are due to the energy loss difference of the backscattered ions of titanium and iron, respectively.

A supplementary analysis of X-ray diffraction was done to know the crystallinity of the samples and to distinguish the thin film prepared at 550 and 600°C. Fig. 4 shows the obtained XRD patterns. At 550°C, the TiFe phase appears (halo diffusion) but does not seem well crystallized. A new phase, $FeTiSi_2$, appeared at 600°C. This is surely due to an inter-diffusion between the Si substrate and the TiFe layer. Hence, to avoid this inter-diffusion, choosing 550°C as the substrate temperature was preferable.

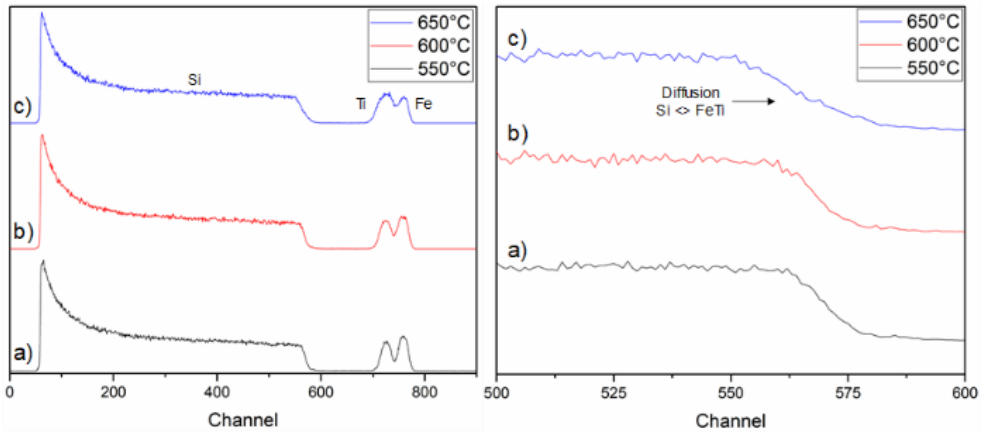

Figure 3. RBS spectra of TiFe layer on Si substrate at (a) 550°C, (b) 600°C, and (c) 650°C (on the left). Zoom is shown on the right.

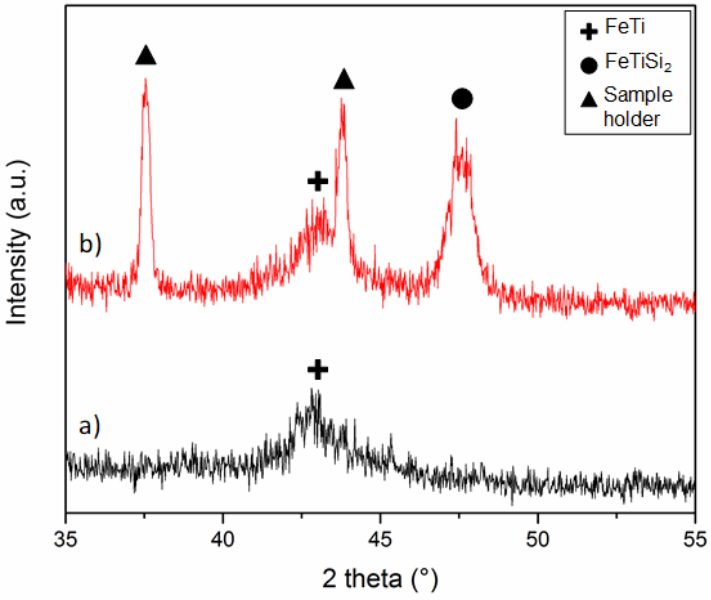

Figure 4. XRD pattern (Bragg-Brentano geometry) of the TiFe layer deposited at a) 550°C and b) 600°C.

3.3. Characterizations of the model system.

3.3.1. Reflectometry experiments.

Neutron reflectometry was used to study the hydrogen (deuterium) absorption in the model system Si/TiFe/Zr/Pd. Fig. 5 shows the typical neutron reflectivity (NR) curves of the sample Si/60 nm TiFe /10 nm Zr /5 nm Pd as prepared, under 10 mbar and 500 mbar of deuterium. The curve exhibits the characteristic Kiessig fringes associated with multiple reflections. The NR curve is quite the same, even if the pressure is increased. There are no significant changes in the tri-layers TiFe/Zr/Pd at the interface between TiFe and Zr. The process of hydrogenation did not occur at this interface. Different chemical analyses were done to understand this observation.

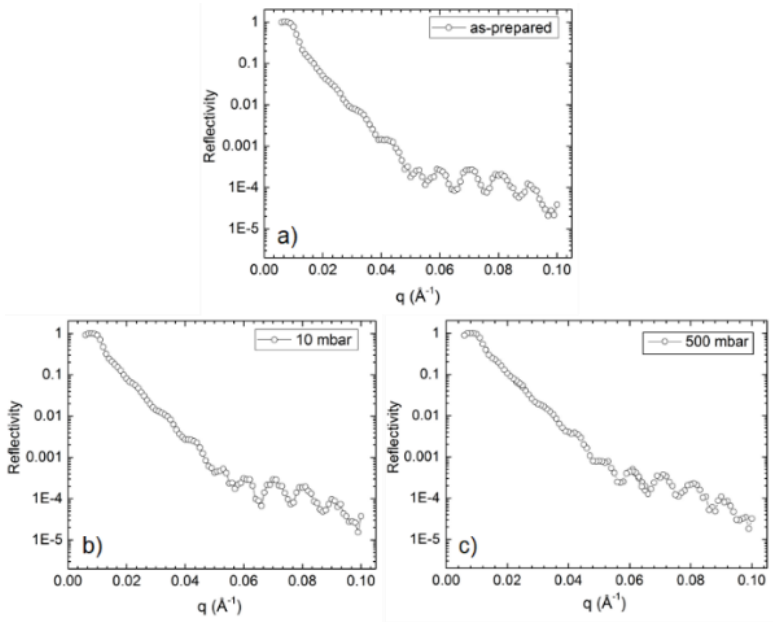

Figure 5. Neutron reflectivity curves for (a) the as-prepared sample, (b) under 10 mbar of deuterium, and (c) under 500 mbar of deuterium.

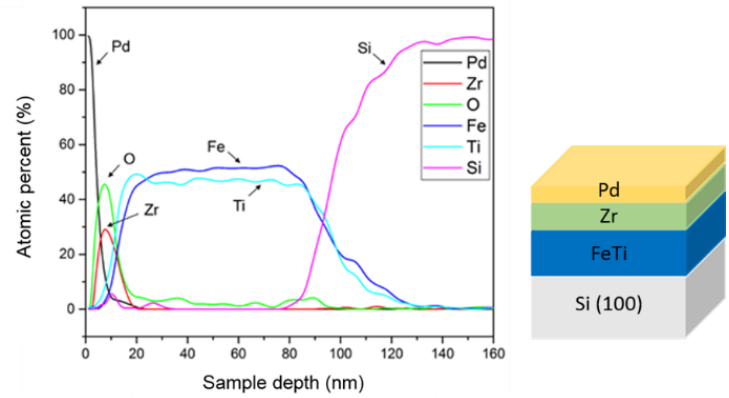

Figure 6. Auger spectra of the tri-layer Pd/Zr/TiFe on a Si wafer and its representation.

3.3.2. Chemical experiments.

Auger electron spectroscopy was used to confirm each layer's chemical composition and thickness. The sputtering rate was 0.04 nm/s. Figure 6 presents the Auger spectra for the Si(100)/TiFe/Zr/Pd model system. The thickness of Fe and Ti layers corresponds to the nominal value (60 nm) with a variation of ± 10 nm.

The palladium covers the sample with a thickness of 5 nm. The correct proportion between Fe and Ti is observed for the whole thickness (*i.e.*, 60 nm). The main problem is the apparition of oxygen during zirconium deposition. Oxygen content rises to 45 %at. or even 60 %at. in some samples. It is surprising that under the same deposition condition, Ti had not formed oxide (as Ti is known as a getter). A transfer machine in the air may be due to the oxidation with air at the sample's surface. However, the transfer time is so short that there should not be such a percentage of oxygen. Then, to avoid this hypothesis, a multilayer Si/TiFe/Zr/TiFe/Zr/Pd was elaborated in the same deposition condition. Fig. 7 presents the Auger analysis of the multilayer. Oxygen is observed in the zirconium layer close to the surface and in the interlayer between the two layers of TiFe. This result suggests that zirconium itself is oxidized.

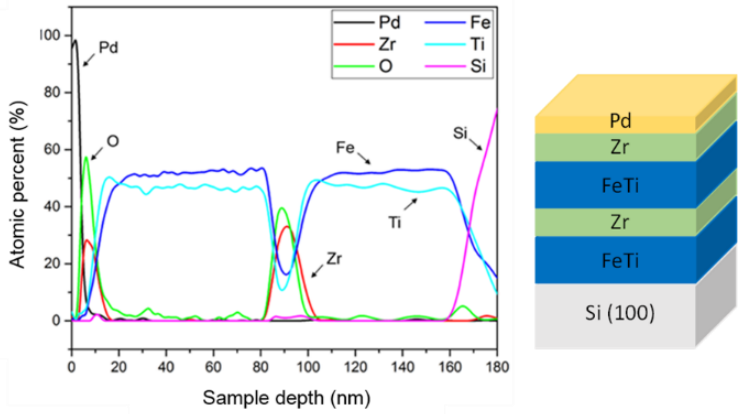

Figure 7. Auger spectra of the multilayer Pd/TiFe/Zr/TiFe on a Si wafer and its representation.

Interphase of 30 nm is observed between the Si substrate and TiFe layer with a composition of $Fe_xTi_xSi_{1-2x}$.

To confirm the bonding between zirconium and oxygen, X-ray photoelectron spectroscopy (XPS) was done with a sputtering rate of 0.2 nm/s. Fig. 8 represents the line shape analysis of XPS core lines of Zr3d, O1s, and Pd3p obtained for the multilayer Pd/Zr/TiFe/Zr/TiFe/Si. For visual clarity, pair of Zr3d emission peaks for every component in the measured Zr3d XPS spectrum is represented by combined doublet features, and both $Zr3d_{3/2}$ and $Zr3d_{5/2}$ were labeled in Fig. 8. Pd3p and O1s peaks are closed in energy, so it can be difficult to distinguish each other. The evolution of the Zr3d peak with etching time was analyzed. The obtained valence state of Zr is +4, which corresponds to the stoichiometric oxide ZrO_2. With a correlation between this evolution and the evolution of the oxygen O1s Auger peak, we confirmed that the zirconium and oxygen were chemically bounded.

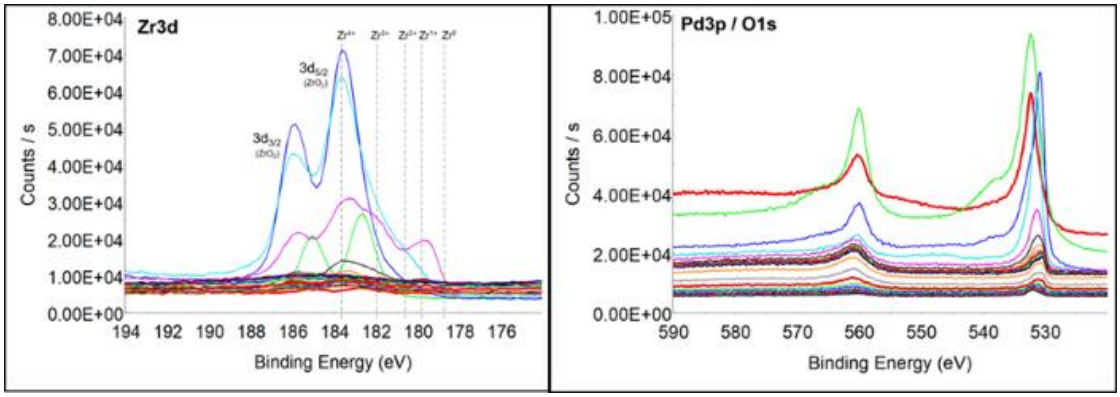

Figure 8. Line shape analysis of XPS core lines of Zr3d, O1s, and Pd3p obtained for a multilayer Pd/Zr/TiFe/Zr/TiFe/Si.

Thus, the zirconium oxidation is most likely responsible for the non-absorption of deuterium. It is well known that an oxide layer acts as a diffusion barrier for hydrogen (deuterium) atoms. The source of oxygen is probably from either the sputtering chamber itself or the Zr target (even if we change the target and make a long time (up to 3 hours) pre-sputtering on it).

3.3.3. Structural experiment.

The grazing incidence X-ray diffraction permits to characterize of the surface of the thin film. The X-ray diffraction pattern of the tri-layer TiFe/Zr/Pd on Si (100) wafer at different incident angles is shown in Fig. 9. For a sample prepared with a substrate temperature of 550°C. At the low angle of 0.3°, *i.e.*, a depth of 12.4 nm, a clear Pd signal is observed, and no signal for TiFe can be detected. This implies that the Pd layer fully covers the TiFe. However, no Zr signal is observed. This probably means that the layer is amorphous at this scale (nm). This amorphization might be due to the presence of oxygen. At the higher angle of 0.6°, it is confirmed that the TiFe is formed with a CsCl structure and its signal increase with the incident angle. For the other multilayer, we did not measure at a higher angle than 1.0° because the substrate signal is too important compared to the other element. Moreover, these spectra indicate that no formation of Fe-Ti-Si compounds occurs, showing that the atomic inter-diffusion between the substrate and TiFe layer is negligible, as shown previously.

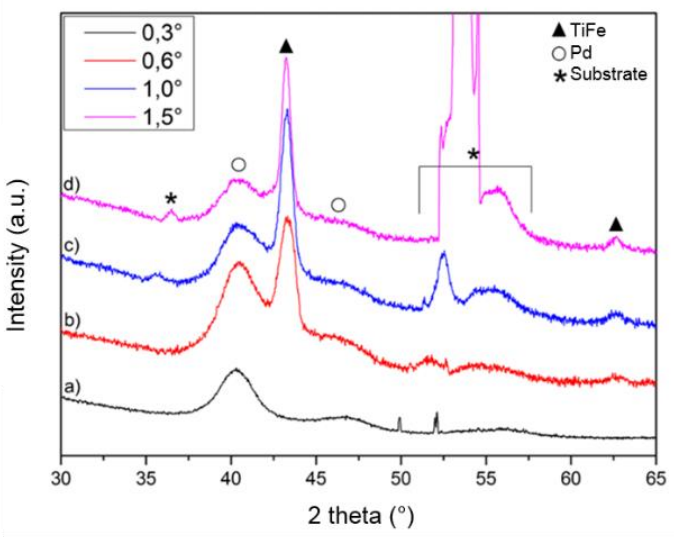

Figure 9. Grazing incidence XRD pattern at a) 0.3°, b) 0.6°, c) 1.0° and d) 1.5° of the multilayers TiFe/Zr/Pd on Si (100) wafer. JCPDS TiFe #03-065-9140.

4. Conclusions

TiFe thin film needs to be synthesized by co-sputtering mode. In addition, depending on the sputtering parameters, and especially the power per unit and substrate temperature, a big variation of composition and crystallization can be obtained. It is necessary to have a substrate temperature of 550°C to obtain a crystallized TiFe thin film without the formation of $FeTiSi_2$. Above this temperature, interdiffusion between the Si substrate and TiFe layer was observed. Also, XPS and Auger spectroscopy highlighted the presence of oxygen and its bounding with zirconium. The presence of an oxide plays the role of a diffusion barrier of hydrogen/deuterium in the multilayer.

Funding

This research received no external funding.

Acknowledgments

This research has no acknowledgment.

Conflicts of Interest

The authors declare no conflict of interest.

References

1. Reilly, J.J.; Wiswall, R.H. Formation and properties of iron titanium hydride. *Inorganic Chemistry* **1974**, *13*, 218-222, https://doi.org/10.1021/ic50131a042.
2. Choong-Nyeon, P.; Jai-Young, L. The activation of FeTi for hydrogenation. *Journal of the Less Common Metals* **1984**, *96*, 177-182, https://doi.org/10.1016/0022-5088(84)90193-0.
3. Jai-Young, L.; Park, C.N.; Pyun, S.M. The activation processes and hydriding kinetics of FeTi. *Journal of the Less Common Metals* **1983**, *89*, 163-168, https://doi.org/10.1016/0022-5088(83)90262-X.
4. Schlapbach, L.; Riesterer, T. The activation of FeTi for hydrogen absorption. *Applied Physics A* **1983**, *32*, 169-182, https://doi.org/10.1007/BF00820257.
5. Heller, E.M.B.; Suyver, J.F.; Vredenberg, A.M.; Boerma, D.O. Oxidation and annealing of thin FeTi layers covered with Pd. *Applied Surface Science* **1999**, *150*, 227-234, https://doi.org/10.1016/S0169-4332(99)00248-2.
6. Jang, T.H.; Han, J.I.; Jai-Young, L. Effect of substitution of titanium by zirconium in TiFe on hydrogenation properties. *Journal of the Less Common Metals* **1986**, *119*, 237-246, https://doi.org/10.1016/0022-5088(86)90684-3.
7. Lee, S.M.; Perng, T.P. Effect of the second phase on the initiation of hydrogenation of TiFe1−xMx (M = Cr,Mn) alloys. *International Journal of Hydrogen Energy* **1994**, *19*, 259-263, https://doi.org/10.1016/0360-3199(94)90095-7.
8. Lim, S.H.; Jai-Young, L. The effects of aluminium substitution in TiFe on its hydrogen absorption properties. *Journal of the Less Common Metals* **1984**, *97*, 65-71, https://doi.org/10.1016/0022-5088(84)90009-2.
9. Lv, P.; Huot, J. Hydrogen storage properties of Ti0.95FeZr0.05, TiFe0.95Zr0.05 and TiFeZr0.05 alloys. *International Journal of Hydrogen Energy* **2016**, *41*, 22128-22133, https://doi.org/10.1016/j.ijhydene.2016.07.091.
10. Oguro, K.; Osumi, Y.; Suzuki, H.; Kato, A.; Imamura, Y.; Tanaka, H. Hydrogen storage properties of TiFe1−xNiyMz alloys. *Journal of the Less Common Metals* **1983**, *89*, 275-279, https://doi.org/10.1016/0022-5088(83)90280-1.
11. Nagai, H.; Kitagaki, K.; Shoji, K. Microstructure and hydriding characteristics of FeTi alloys containing manganese. *Journal of the Less Common Metals* **1987**, *134*, 275-286, https://doi.org/10.1016/0022-5088(87)90567-4.
12. Nagai, H.; Kitagaki, K.; Shoji, K.I. Hydrogen Storage Characteristics of FeTi Containing Zirconium. *Transactions of the Japan Institute of Metals* **1988**, *29*, 494-501.
13. Heller, E.M.B.; Vredenberg, A.M.; Boerma, D.O. Hydrogen uptake kinetics of Pd coated FeTi films. *Applied Surface Science* **2006**, *253*, 771-777, https://doi.org/10.1016/j.apsusc.2006.01.004.
14. Jain, P.; Gosselin, C.; Huot, J. Effect of Zr, Ni and Zr7Ni10 alloy on hydrogen storage characteristics of TiFe alloy. *International Journal of Hydrogen Energy* **2015**, *40*, 16921-16927, https://doi.org/10.1016/j.ijhydene.2015.06.007.
15. Suzuki, R.; Ohno, J.; Gondoh, H. Effect of sulphur addition on the properties of Fe ·Ti alloy for hydrogen storage. *Journal of the Less Common Metals* **1984**, *104*, 199-206, https://doi.org/10.1016/0022-5088(84)90455-7.
16. Abe, M.; Kuji, T. Hydrogen absorption of TiFe alloy synthesized by ball milling and post-annealing. *Journal of Alloys and Compounds* **2007**, *446-447*, 200-203, https://doi.org/10.1016/j.jallcom.2006.12.063.
17. Emami, H.; Edalati, K.; Matsuda, J.; Akiba, E.; Horita, Z. Hydrogen storage performance of TiFe after processing by ball milling. *Acta Materialia* **2015**, *88*, 190-195, https://doi.org/10.1016/j.actamat.2014.12.052..
18. Aoyagi, H.; Aoki, K.; Masumoto, T. Effect of ball milling on hydrogen absorption properties of FeTi, Mg2Ni and LaNi5. *Journal of Alloys and Compounds* **1995**, *231*, 804-809, https://doi.org/10.1016/0925-8388(95)01721-6.

19. Chen, Y.; Williams, J.S. Formation of metal hydrides by mechanical alloying. *Journal of Alloys and Compounds* **1995**, *217*, 181-184, https://doi.org/10.1016/0925-8388(94)01338-1.
20. Zaluski, L.; Zaluska, A.; Tessier, P.; Ström-Olsen, J.O.; Schulz, R. Catalytic effect of Pd on hydrogen absorption in mechanically alloyed Mg2Ni, LaNi5 and FeTi. *Journal of Alloys and Compounds* **1995**, *217*, 295-300, https://doi.org/10.1016/0925-8388(94)01358-6.
21. Vredenberg, A.M.; Heller, E.M.B.; Boerma, D.O. Hydriding characteristics of FeTi/Pd films. *Journal of Alloys and Compounds* **2005**, *400*, 188-193, https://doi.org/10.1016/j.jallcom.2005.03.081.
22. Fritzsche, F.K.H.; Rehm, C.; Tun, Z.; Wolff, M.; Hjörvarsson, B. Neutron reflectometry. In: *Neutron scattering and other nuclear techniques for hydrogen in materials.* ed: Springer, **2016**; pp. 115-158.
23. Razafindramanana, V.; Gorsse, S.; Huot, J.; Bobet, J.L. Effect of Hafnium Addition on the Hydrogenation Process of TiFe Alloy. *Energies* **2019**, *12*, https://doi.org/10.3390/en12183477.